Applied Physics Letters

Study on nonlinear magnetic droplets in a flow-focusing generator

Cite as: Appl. Phys. Lett. **115**, 031903 (2019); https://doi.org/10.1063/1.5104296
Submitted: 26 April 2019 . Accepted: 29 June 2019 . Published Online: 17 July 2019

Jie Wu, Lei Pei, Xiaokang He, Yiwen Cui, Shouhu Xuan, and Xinglong Gong

View Online Export Citation CrossMark

Lake Shore CRYOTRONICS
Sensors, Controllers, Monitors
from the world leader in cryogenic thermometry

AIP Publishing

© 2019 Author(s).

Applied Physics Letters ARTICLE scitation.org/journal/apl

Study on nonlinear magnetic droplets in a flow-focusing generator

Cite as: Appl. Phys. Lett. **115**, 031903 (2019); doi: 10.1063/1.5104296
Submitted: 26 April 2019 · Accepted: 29 June 2019 ·
Published Online: 17 July 2019

View Online Export Citation CrossMark

Jie Wu, Lei Pei, Xiaokang He, Yiwen Cui, Shouhu Xuan,[a] and Xinglong Gong[a]

AFFILIATIONS

CAS Key Laboratory of Mechanical Behavior and Design of Materials, Department of Modern Mechanics, CAS Center for Excellence in Complex System Mechanics, University of Science and Technology of China, Hefei 230027, China

[a]Electronic addresses: xuansh@ustc.edu.cn and gongxl@ustc.edu.cn

ABSTRACT

A nonlinear magnetic droplet in a flow-focusing channel is studied in this letter. The breakup regime of the droplets undergoes a transition from dripping to bifurcation to dripping. A GMR (giant magnetoresistance) sensor is proposed for droplet detection. When this nonlinear droplet passes, the sensor can produce a continuous jitter signal which is significantly different from the one obtained in the dripping mode. The MR (magnetoresistive) ratio is about 3.2%. The droplet magnetic field obtained by molecular dynamics simulation demonstrates that the GMR sensor is effective in the detection.

Published under license by AIP Publishing. https://doi.org/10.1063/1.5104296

Droplet-based microfluidics attracts increasing attention because it can accurately handle trace amounts of fluid elements.[1] Specifically, magnetic droplets in immiscible oil have a variety of applications in biology and engineering, such as drug delivery,[2] cell sorting,[3] magnetic separation,[4] and pumps and valves.[5] T-junction, coflow, and flow-focusing are the most commonly used microfluidic methods for droplet generation.[6] A flow-focusing generator can provide highly uniform droplets to ensure constant, controlled, and predicted results. However, droplet generation originates from fluid instabilities.[7] Magnetic droplets can be generated by introducing magnetic fluid as dispersed fluid into another continuous fluid, and their generation modes include squeezing, dripping, jetting, and thread formation.[8] The competition of inertia force, interfacial tension force, and capillary force determines the specific breakup regime of droplet generation. In addition, the magnetic fluids can be magnetized under the action of the external field, and thus, the changed viscosity and surface tension exhibit a more complicated situation.

Moreover, magnetoresistive (MR) sensors have been successfully applied to the field of droplet-based microfluidics,[9–13] showing good magnetic field detection capabilities. The concept of magnetic droplet editing, decoding,[9,10] and size monitoring[12] in a microfluidic platform has been proposed by GMR (giant magnetoresistance) sensors. GMR sensors have a very high sensitivity, but at the same time, they enter saturation at very low magnetic fields.[14] Although the colocation monitoring of droplets has been involved, the magnetic field strength generated by a single superparamagnetic droplet under the action of an external magnetic field has hardly been explored. In particular, a weak magnetic field can cause sensor saturation.

Here, a long orifice throat flow-focusing chip was used to generate magnetic droplets. Nonlinear droplets were found at a certain flow rate ratio. A high-speed camera (Phantom V2512) was utilized to record the entire generation process of magnetic droplets. A high MR ratio GMR sensor was used to characterize the droplet modality. The sensor responded to weak magnetic fields and was quickly saturated. When a droplet flowed through the magnetic sensitive region, the superparamagnetic particles dispersed therein were magnetized by the external magnetic field. Molecular dynamics was used to simulate the magnetic fields which were generated by magnetic droplets of 50 μm and 60 μm (the diameter of droplets), respectively. A magnetic field opposite to the direction of the excitation field was generated in the magnetosensitive area. A suitable external magnetic field was chosen to ensure the sensor is operated in a good magnetic field response segment. This work will be of great significance for guiding the detection of paramagnetic samples in a magnetoresistive microfluidic system.

Figure 1(a) shows the polydimethylsiloxane (PDMS, Sylgard 184, Dow Corning) device fabricated through a standard soft-lithography technique.[15] Two high-precision syringe pumps (LSP02–1B, LongerPump) pump magnetic fluid and mineral oil (Sigma-Aldrich) into the flow-focusing chip [Fig. 1(b)]. Superparamagnetic Fe_3O_4 particles (solvothermal method[17]) were dispersed in de-ionized water to obtain the magnetic fluid. Two immiscible fluids encounter at the intersection, and high-frequency magnetic droplets are generated by the large capillary number caused by the long orifice. The camera was utilized to record the droplet mode at different flow rate ratios. The volume flow rate of magnetic fluid was fixed at 0.1 ml/h, while increasing the

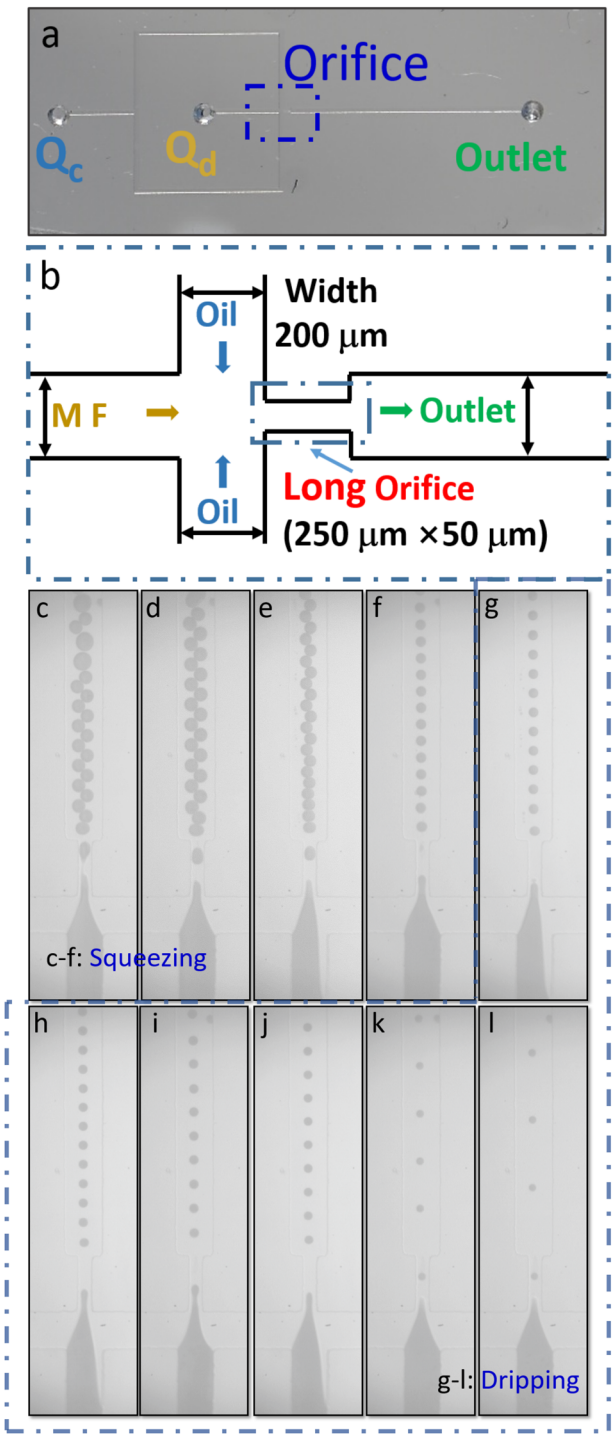

FIG. 1. (a) The plane map of the flow-focusing channel. (b) Dimensional description of the earth part of the channel. The widths of the continuous phase (mineral oil), dispersed phase (magnetic fluid), and outlet are all 200 μm. The long orifice is 250 μm× 50 μm. (c)–(l) The transition of magnetic droplets. Q_d was 0.1 ml/h, and Q_c was increased from 0.1 ml/h to 1.0 ml/h. The droplet modes changed from squeezing [(c)–(f)] to dripping [(g)–(l)].

continuous phase flow rate was varied from 0.1 ml/h to 1.0 ml/h. Figures 1(c)–1(l) show the mode transition of magnetic droplets by changing a two-phase flow ratio from 1:1 to 1:10. As the flow rate ratio increased, the size of droplets decreased and generation frequency increased. The entire formation of the droplets was carefully observed (with or without shrinkage at the magnetic fluid tip) at each flow rate, and the droplet mode changed from "squeezing" to "dripping."

Surprisingly, this long orifice flow-focusing device produces a particular mode of droplets. Figures 2(a)–2(p) display the generation process of the nonlinear droplets. By increasing the Q_d to 0.15 ml/h slightly, "Bifurcation" [Fig. 2(r)] occurred in the range of dripping modes [Figs. 2(q)–2(s)], of which Q_c was kept at 0.18 ml/h, 0.30 ml/h, and 0.60 ml/h, respectively. Figures 2(a)–2(p) show the whole process of the bifurcation droplets recorded with the camera frame rate of 10 000. Except for uniform droplets, a primary droplet followed by a small secondary droplet was periodically present, and the magnetic fluid tip in the orifice did not shrink. According to the time interval between figures, one primary droplet is generated every 3 ms [Figs. 2(a)–2(k)], and then, the secondary droplet is generated in 1.5 ms [Figs. 2(l)–2(p)]. Since the flow rate is fixed and the liquid is incompressible, the total volume of the primary and secondary droplets is about 188 pl, and the diameters of these two droplets are 62 μm and 49 μm, respectively. In the experiments, we found that bifurcation occurred in a fairly large flow rate range. Different from conventional higher-order periods and the chaotic bubbling phenomenon which typically occurred in a high Weber number (We), this dripping to bifurcation to dripping transition is acquired at a low flow rate. Unlike water-in-oil droplets under traditional optical observations, magnetoresistive sensors can also be used to characterize magnetic droplets in microfluidics. As the droplets flow through the magnetic sensitive region, the resulting magnetic field will be recorded by the GMR sensor.

Therefore, a GMR sensor was designed and fabricated for characterizing magnetic droplets. The fabrication contains a total of two

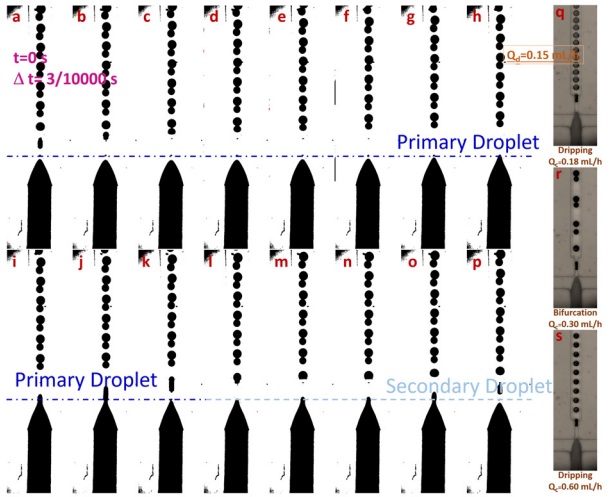

FIG. 2. (a)–(p) The whole generation process of the bifurcation droplet. The camera frame rate is 10 000, and the interval between adjacent figures is 3/10 000 s. (a)–(k) The primary droplet is followed by the (l)–(p) secondary droplet. Q_d is fixed at 0.15 ml/h. Q_c is increased from (q) 0.18 ml/h to (r) 0.30 ml/h to (s) 0.60 ml/h, and the droplet mode transits from (q) dripping to (r) bifurcation to (s) dripping again.

Published under license by AIP Publishing

lift-off processes. Figure 3 details the method of sensor manufacture. This multilayer thin film magnetosensitive body is $[Ni_{81}Fe_{19}/Cu]_{30}$. The first photolithography was to obtain a tortuous magnetic zone pattern [the right side of Fig. 3(f)]. Each rectangle is 100 μm × 3 μm, and the spacing is 3 μm. With the help of the mask alignment marks, the second lift-off process resulted in the sensor electrodes.

The outlet of the flow-focusing chip was aligned with the magnetosensitive area and then bonded to the sensor. Figure 4(a) shows the obtained device, and Fig. 4(b) shows the optical microscopy image of the GMR sensor. The bend line in the figure is the magnetosensitive area. A single magnetic enthalpy and impedance meter (Modulab MTS) was used to characterize the magnetic field response of the sensor. As the magnetic field acting on the magnetosensitive area increases from 0 to 220 Oe, the resistance of the sensor first decreases and then remains almost unchanged [Fig. 4(c)]. The initial resistance of the sensor is 1118.4 Ω and the maximum variation over the whole process is 35.8 Ω, and thus, the MR ratio is about 3.2%. Therefore, the sensor is sensitive to a weak magnetic field, and the saturation magnetic field is about 150 Oe. Therefore, the total magnetic field acting on the magnetosensitive area should be less than this value. The magnetic properties of superparamagnetic particles in the droplet should be magnetized by the external magnetic field. From the MR sensitivity curve in Fig. 4(c), it can be concluded that the sensor increased from a high sensitivity resolution to a linear response to the saturation phase as the magnetic field increased.

For superparamagnetic samples, a suitable external excitation field is critical to the effective operation of the GMR sensor. If the excitation magnetic field is too small, it is difficult for the particles in the droplet to form chainlike structures. Molecular dynamics is used to simulate the magnetic field generated by a microdroplet. The diameters of the magnetic droplets are 50 and 60 μm, respectively, and the particle mass fraction is 10 wt. %. When the Fe_3O_4 particle is subjected to an external magnetic field $\boldsymbol{H}$, the magnetic moment vector $\boldsymbol{m_i}$ can be expressed as

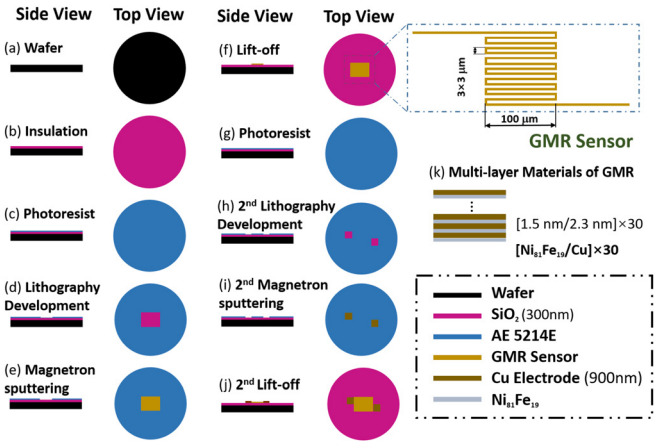

FIG. 3. Schematic diagram of GMR sensor processing. Sputtering 600 nm thick SiO_2. (b) Insulating layer on the surface of (a) a 2 in. wafer. (c) Coating AE 5124E photoresist, (d) lithography (Optical Aligner-SUSS MABA6), development (AZ 300 MIF), and obtained pattern area. (e) and (f) Sputter multilayer thin film metal (Lesker Lab18) and lift-off the unetched photoresist. (g)–(j) Repeating the same process obtains the electrodes.

$$\boldsymbol{m}_i = MV_i\frac{\boldsymbol{H}}{H} = M_s e^{-\frac{C_1}{H+C_2}}V_i\frac{\boldsymbol{H}}{H}, \tag{1}$$

where M is the magnetization of Fe_3O_4 and V_i is the particle volume. H means the modulus of the magnetic field vector. The saturation magnetization M_s of the particles is 90.7 emu/g. C_1 and C_2 together determine the magnetization characteristics near the zero magnetic field, $C_1 = 330$ Oe and $C_2 = 72.6$ Oe. C_1 measures the speed toward saturation. For this superparamagnetic particle, the Langevin function can be used to describe the magnetic hysteresis loop,[16]

$$M = M_s\left[\coth(x) - \frac{1}{x}\right]. \tag{2}$$

Here, $x = M_s V_p H/k_B T$, where V_p is the average volume of the particle. Under the action of an external magnetic field, functions (1) and (2) can be expressed as

$$M = M_s\left(1 - \frac{C_1}{H}\right) = M_s\left(1 - \frac{k_B T}{M_s V_p H}\right). \tag{3}$$

Near the zero magnetic field, Eqs. (1) and (2) should be able to translate into the same linear relationship with magnetic field strength,

$$\left(\frac{dM}{dH}\right)_{H=0} = \frac{C_1}{C_2}e^{-C_1/C_2} = \frac{M_s V_p}{3k_B T}. \tag{4}$$

It is assumed that all particles in the magnetic fluid are uniformly magnetized instantaneously, and the direction of the magnetic moment is parallel to the direction of the external magnetic field. At the same time, the magnetized particles also generate a magnetic field in the surrounding area,

$$\boldsymbol{H_i} = -\frac{1}{4\pi r^3}[\boldsymbol{m}_i - 3(\boldsymbol{m}_i \cdot \hat{\boldsymbol{r}})\hat{\boldsymbol{r}}], \tag{5}$$

where $\boldsymbol{r}$ is the position vector of the center of the particle i to a certain point. Another particle is present in the magnetic field $\boldsymbol{H_i}$, which is also magnetized by the particle i. After a number of iterative calculations, the magnetization of a single particle can be obtained. Finally, the magnetic moment of a single particle is

$$\boldsymbol{m}_i = M_s e^{-\frac{C_1}{|\boldsymbol{H}_{loc}|+C_2}}V_i\frac{\boldsymbol{H}_{loc}}{H_{loc}}, \tag{6}$$

$$\boldsymbol{H}_{loc} = \boldsymbol{H} + \sum_{j\neq i}\boldsymbol{H}_j. \tag{7}$$

$\boldsymbol{H}_{loc}/H_{loc}$ means the direction of magnetic moment vector. Equation (7) applies the superposition principle. This makes it possible to obtain the magnetization state of the droplets under the action of a weak magnetic field. Figure 4(e) shows the distribution of the particles in the droplet. The external magnetic field is 100 Oe, and the direction is along the z-axis. The resulting particle distribution is rotated by a certain angle for easy observation. The particles form chain-like structures along the magnetic field direction.

It can be seen from the droplet monitoring system [Fig. 4(d)] that the sensor is located at the plane out of the droplet edge. Figure 4(f) first shows the response of GMR sensor's resistance value as the random microdroplet passes. Different size troughs indicate the passage of droplets of different diameters. Then, the calculations gave the

Published under license by AIP Publishing

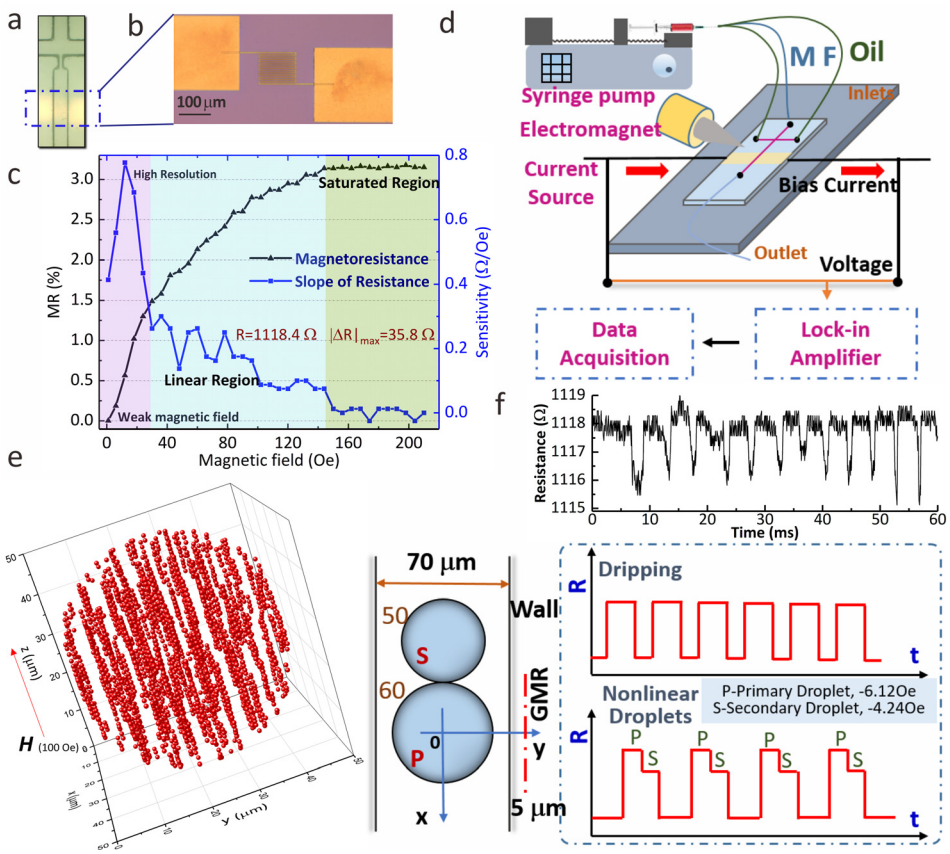

FIG. 4. (a) Map of the flow-focusing chip bonded to (b) the GMR sensor. (c) MR ratio and sensitivity versus the magnetic field acting on the magnetosensitive area. The response relationship is divided into three parts. (d) Schematic of the droplet monitoring system. (e) Superparamagnetic particle distribution in a droplet with a diameter of 50 μm under the action of 100 Oe magnetic field. The z-axis is aligned with the direction of the external magnetic field and parallel to the channel and sensor plane. (f) Experimental and schematic response of the GMR sensor to the micromagnetic droplets.

magnetic fields generated by a 50 μm droplet located at the x-z planes of 55 μm, 60 μm, and 65 μm. They are −12.04 Oe, −6.63 Oe, and −4.24 Oe, respectively. The negative sign indicates that the direction of these magnetic fields is opposite to the external magnetic field. The 60 μm droplet exhibits a similar situation. For the x-z planes of 65 μm, 70 μm, and 75 μm, they are −8.86 Oe, −6.12 Oe, and −4.36 Oe, respectively. The larger droplet corresponds to the smaller magnetic field for the farther center distance. For this flow-focusing device, the magnetic field at the same distance (35 μm) from the center of the droplets is −6.63 Oe and −8.86 Oe. The 60 μm droplet produces a magnetic field that is about 33.6% higher than that of the 50 μm droplet. Due to the uniformity of the dripping mode droplets, a periodic signal response is generated in the sensor [Fig. 4(f)]. However, based on the molecular dynamics simulation, the periodic, continuous, and jittery signal corresponds to the nonlinear droplet. Under the excitation of a weak external magnetic field, a weaker magnetic field generated by the paramagnetic materials is sufficient to be recorded by the sensor. Moreover, the nonlinear droplet can produce significantly different signals at the sensor.

In this letter, a bifurcated magnetic droplet in a long orifice flow-focusing generator was described. A high speed camera was utilized to record the entire formation process of primary and secondary droplets. Such a nonlinear magnetic droplet phenomenon occurred in the dripping mode. To facilitate the characterization of the GMR sensor, the particle distribution in the droplets under the application of a weak magnetic field was analyzed by molecular dynamics simulation. The magnetic field produced by the droplet acting on the magnetosensitive area was within the response accuracy of the GMR sensor. This work is of great significance for the study of paramagnetic materials in magnetoresistive microfluidic chip systems.

Financial support from the National Natural Science Foundation of China (Grant Nos. 11572310, 11572309, and 11822209) is gratefully acknowledged. This study was also supported by the Collaborative Innovation Center of Suzhou Nano Science and Technology. This work was partially carried out at the USTC Center for Micro- and Nanoscale Research and Fabrication.

REFERENCES

[1]S. Y. Tang, K. Wang, K. Fan, Z. L. Feng, Y. X. Zhang, Q. B. Zhao, G. L. Yun, D. Yuan, L. M. Jiang, M. Li, and W. H. Li, Anal. Chem. **91**, 3725 (2019).
[2]T. H. Nguyen, X. Chen, A. Sedighi, U. J. Krull, and C. L. Ren, Microfluid. Nanofluid. **22**, 63 (2018).
[3]Y. J. Sung, J. Y. H. Kim, H. I. Choi, H. S. Kwak, and S. J. Sim, Sci. Rep. **7**, 10390 (2017).
[4]U. Banerjee, A. Raj, and A. K. Sen, Appl. Phys. Lett. **113**, 143702 (2018).
[5]Z. Han, W. Li, Y. Huang, and B. Zheng, Anal. Chem. **81**, 5840 (2009).
[6]P. Zhu and L. Wang, Lab Chip **17**, 34 (2017).
[7]P. Garstecki, H. A. Stone, and G. M. Whitesides, Phys. Rev. Lett. **94**, 164501 (2005).
[8]W. Lee, L. M. Walker, and S. L. Anna, Phys. Fluids **21**, 032103 (2009).
[9]W. Song, G. Lin, J. Ge, J. Fassbender, and D. Makarov, ACS Sens. **2**, 1839 (2017).

Published under license by AIP Publishing

[10]G. Lin, D. Makarov, M. Medina-Sanchez, M. Guix, L. Baraban, G. Cuniberti, and O. G. Schmidt, Lab Chip **15**, 216 (2015).
[11]G. Lin, V. M. Fomin, D. Makarov, and O. G. Schmidt, Microfluid. Nanofluid. **19**, 457 (2015).
[12]N. Pekas, M. D. Porter, M. Tondra, A. Popple, and A. Jander, Appl. Phys. Lett. **85**, 4783 (2004).
[13]J.-Y. Hong, S.-H. Chang, K.-H. O. Yang, P.-C. Yeh, H.-W. Shiu, C.-H. Chen, W.-C. Chiang, and M.-T. Lin, J. Appl. Phys. **125**, 142905 (2019).
[14]S. Cardoso, D. C. Leitao, T. M. Dias, J. Valadeiro, M. D. Silva, A. Chicharo, V. Silverio, J. Gaspar, and P. P. Freitas, J. Phys. D: Appl. Phys. **50**, 213001 (2017).
[15]D. C. Duffy, J. C. McDonald, O. J. A. Schueller, and G. M. Whitesides, Anal. Chem. **70**, 4974 (1998).
[16]S. Xuan, F. Wang, Y.-X. J. Wang, J. C. Yu, and K. C.-F. Leung, J. Mater. Chem. **20**, 5086 (2010).
[17]B. D. Cullity and C. D. Graham, *Introduction to Magnetic Materials* (John Wiley & Sons, 2011).

Published under license by AIP Publishing